Title

Pilot-scale NO x removal efficacy of photocatalytic roofing granules under urban environmental conditions

Authors

Tang, Xiaochen
Ughetta, Lara
Gould, Rachael AT
et al.

Publication Date

2022-10-01

DOI

10.1016/j.solmat.2022.111907

Solar Energy Materials & Solar Cells 247 (2022) 111907

Contents lists available at ScienceDirect

Solar Energy Materials and Solar Cells

journal homepage: www.elsevier.com/locate/solmat

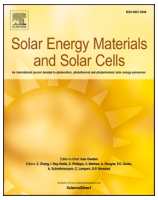

Pilot-scale NO_x removal efficacy of photocatalytic roofing granules under urban environmental conditions

Xiaochen Tang [a,*], Lara Ughetta [b], Rachael A.T. Gould [b], Rebecca L.A. Everman [b], Taisiya Skorina [b], Sharon Chen [a], Maureen Kavanagh [b], Ronnen Levinson [a], Hugo Destaillats [a,*]

[a] Energy Technologies Area, Lawrence Berkeley National Laboratory, 1 Cyclotron Road, Berkeley, CA, 94720, USA
[b] Industrial Mineral Products Division, The 3M Company, 3M Center, Building 209, 1-W-14, St. Paul, Minnesota, 55144, USA

ARTICLE INFO

Keywords:
Building envelope
TiO_2
NO_x
de-pollution
Pilot scale

ABSTRACT

Photocatalytic building envelope materials harness sunlight to activate self-cleaning and de-polluting properties, which can help mitigate the urban heat island effect and abate urban pollution. The performance of roofing membranes manufactured with bright-white photocatalytic (BWP) granules, and with a non-photocatalytic bright-white control (BWC), were evaluated. The solar reflectance of unexposed specimens was 0.56 for BWP and 0.60 for BWC. Small changes in solar reflectance with respect to the initial values were observed during 22 months of field exposure between March 2020 and January 2022, indicating good resistance to soiling. Changes in the de-pollution capacity during the same period were quantified with a bench-scale method adapted from the ISO Standard 22197-1, in which unexposed and aged specimens were placed horizontally inside a flow chamber admitting clean air enriched with nitric oxide (NO) under UV irradiation. In addition, a pilot-scale approach was developed to evaluate the photocatalytic performance of the same materials under more realistic urban environmental conditions. An outdoor exposure chamber was designed and built with a rectangular stainless-steel main body topped with a UV-transparent fluorinated ethylene propylene (FEP) thin film. The area of the 30 cm × 90 cm BWP specimen tested in the outdoor chamber was more than one order of magnitude larger than those evaluated in the benchtop apparatus. The BWP membrane was pre-activated by field exposure for 75 days. The pilot-scale chamber operation was validated in the laboratory using UV lamps to irradiate the BWP membrane and a reference TiO_2-coated aluminum plate (P25, 1 g m^{-2}) of the same dimensions. Tests showed comparable or better performance of the BWP membrane with respect to the P25 film. Its de-pollution capacity was tested with direct sunlight irradiation in Berkeley, California (37.88° N, 122.25° W) during June 2020. Urban air was enriched with NO, or with a NO/NO_2 mixture, and circulated through the pilot-scale chamber at two different flows: 1.1 and 440 L min^{-1}. The gas phase concentrations of NO and NO_2 were measured upstream and downstream of the tested specimen with a chemiluminescence analyzer. Upstream levels of the challenge gases were high but realistic, not exceeding 200 ppb. The UV irradiance outdoors (15–30 W m^{-2}) was higher and more variable than in indoor tests (11.5 W m^{-2}), leading to overall higher NO deposition velocity under direct sunlight. In outdoor measurements, the NO deposition velocity increased at higher irradiances. When NO was the only challenge gas, a fraction of NO was oxidized to NO_2 resulting in lower NO and higher NO_2 downstream concentrations. However, when tested with NO/NO_2 mixtures, the concentration of both compounds decreased during irradiation, and the surface showed a faster loss of photoactivity for NO_2, compared with NO. These effects are consistent with those observed in the laboratory. The NO_x deposition velocity outdoors was 0.7 and 105 μmol h^{-1} m^{-2} for the low and high air flow, respectively.

1. Introduction

Photocatalytic building envelope materials are of interest due to their ability to harness sunlight to activate self-cleaning and de-polluting effects. Examples of their applications have been reported for prototype roofing materials such as tiles, shingles, and acrylic coatings [1–4]. Similarly, photocatalytic wall materials include cementitious coatings, limestone treatments and composite siding [5–8]. De-polluting

* Corresponding authors.
E-mail addresses: XTang@lbl.gov (X. Tang), HDestaillats@lbl.gov (H. Destaillats).

https://doi.org/10.1016/j.solmat.2022.111907
Received 24 March 2022; Received in revised form 12 July 2022; Accepted 18 July 2022
Available online 29 August 2022

performance of these materials has traditionally been studied in the laboratory with a bench-scale test method. For example, our group has evaluated in bench-scale tests the ability of photocatalytic roofing granules to eliminate from air the nitrogen oxides NO and NO_2 (commonly referred to as $NO + NO_2 = NO_x$) [9]. The same approach was also used to assess the de-NO_x efficiency of photocatalytic architectural fabrics [10]. Photocatalytic removal of volatile organic compounds (VOCs) and other inorganic pollutants (e.g. SO_2) has also been studied for cementitious materials [11], silicate coatings [12], TiO_2 films and nanoparticles [13,14], and paints [15]; the overall progress has been reviewed several times in the past decade [16–19]. Another application of photocatalytic materials is to use their high solar reflectance and self-cleaning capabilities to mitigate the urban heat island (UHI) effect [20–23].

Initial evaluation of photocatalytic materials is often carried out with standardized bench-scale tests. One of the most popular methods is the ISO Standard 22197-1 "Fine ceramics (advanced ceramics, advanced technical ceramics) – test method for air purification performance of semiconducting photocatalytic materials. Part 1: Removal of nitric oxide" [24]. In this test, a flat photocatalytic material is placed horizontally inside a flow chamber admitting air enriched with NO under a UV lamp, with continuous monitoring of NO and NO_2 concentration downstream of the chamber. This standardized method is used by many authors to assess photocatalytic activity, allowing for a direct comparison with a growing number of studies [25–30].

While ISO 22197-1 is easy to operate and provides useful information, it is also limited in its ability to predict how a photocatalytic material will perform in real world conditions. Those testing conditions have been optimized to maximize a rapid signal in the laboratory, but are far from how exposure takes place in the environment. The ISO 22197-1 and other methods rely on challenging the tested material with NO, avoiding the presence of NO_2 in the air admitted to the chamber. However, in most urban environments both compounds are present, and NO_2 concentrations are typically higher than those from NO. Further, the NO concentration recommended by the ISO 22197-1 method is 1000 parts per billion (ppb), which is two orders of magnitude higher than levels usually found in urban environments. In the ISO 22197-1 method, the NO is mixed with clean air from a cylinder, rather than with ambient air containing other gaseous and particulate pollutants. Those pollutants co-occur in the environment and can interact with the catalyst surface, influencing the de-NO_x process. Standardized tests are performed in a piston-flow reactor with constant air flow, in conditions that control diffusion to the surface by limiting vertical mixing and convection. However, under real-world conditions mass transfer to the catalytic material is highly variable depending on parameters such as surface tilt angle and meteorological conditions. In ISO 22197-1, experiments are performed at ambient laboratory temperatures (e.g., 25 °C), while building envelope materials exposed to the sun are typically warmer (e.g., 50–80 °C). Bench-scale methods use UV lamps to irradiate the sample continuously, rather than sunlight.

The goal of this study was to develop a testing method at a scale larger than that of ISO 22197-1, to enable systematical evaluation of the photocatalytic performance of prototype photocatalytic roofing materials under realistic ambient conditions. In particular, an outdoor exposure chamber was designed to test specimens that are more than an order of magnitude larger in area than those measured in bench-scale systems. This pilot-scale chamber allowed specimens to be directly exposed to the sun while challenged with urban air enriched in NO, and in a NO/NO_2 mixture. The concentrations of the challenge gases were high but realistic, not exceeding 200 ppb. The pilot chamber operation was tested and validated in the laboratory before it was used in the field. Results were also compared with those obtained with the same materials using the ISO 22197-1 method. The approach was applied to a prototype roofing membrane coated with photocatalytic "bright white" granules.

2. Material and methods

2.1. Preparation of tested materials

The experimental methods were validated using a reference sample, a titanium dioxide (TiO_2)-coated aluminum plate, before being applied to the samples provided by 3M. The sub-sections below describe how the reference and membrane specimens used in bench-scale and pilot-scale tests were prepared and conditioned.

2.1.1. P25 plates

The reference samples were aluminum plates coated with P25 TiO_2 (mixture of anatase and rutile phases, Aeroxide® Evonik, Germany) [31]. The surface coverage was 1 g m^{-2}. In the bench-scale experiment, a 10 cm × 20 cm plate was coated with 20 mg P25 suspended in 8 mL of de-ionized (DI) water, prepared by pre-sonicating for 30 min to fully suspend the catalyst in water. After quantitatively transferring the suspension to the surface, the coated aluminum plate was placed on a heating plate at 60 °C to evaporate water and form a homogeneous layer. Similarly, three 30.5 cm × 30.5 cm (12" × 12") square plates were coated with 93 mg P25 for the pilot-scale experiments.

2.1.2. Roofing membranes

Two types of roofing samples were provided by 3M for the testing: a bright-white photocatalytic (BWP) membrane, and a matching bright-white control (BWC) non-photocatalytic membrane. Two sizes of specimens were provided: 10 cm × 20 cm for the bench-scale test, and 31 × 91 cm (12" × 36") for the pilot-scale evaluation. The membranes comprised an outer layer of bright white granules applied on an asphaltic membrane. The granules comprised a base mineral coated with a reflective ceramic layer, a photocatalytic layer, and an adhesion-promoting silicone coating. The catalyst was dispersed through a silicate binder, and applied to the surface of the granules. The silicate binder formed a semi-ceramic surface coating after being fired at 200–370 °C. More details of the granule coating process are provided in two United States patents [32,33].

BWP and BWC samples were activated through exposure in the outdoor environment on racks mounted on a laboratory roof in Berkeley, California (latitude 37.88°N, longitude 122.25°W). The racks were south-facing, tilted at a 45° angle with respect to the horizon. Large specimens were exposed for 75 days between 2020-03-05 and 2020-05-19, a wet spring with about 7 cm of rain recorded during that period. Small specimens were exposed between 2020-03–05 and 2022-01-05, with individual specimens retrieved at different times during that period. One specimen was retrieved on 2020-06-29, after 116 days of exposure that included the end of the rainy season and the beginning of the dry season. The second specimen was retrieved on 2020-10-26, corresponding to a total of 235 days of exposure, of which the last four months were in the dry season. Two additional specimens were retrieved after 12 months and 22 months of continuous exposure, respectively, to evaluate the effects of long-term weathering. A timeline showing exposure periods and precipitation is shown in Fig. S1 (Supporting Information). At the end of the exposure, all specimens were retrieved from the rack and stored in the dark at room temperature in the laboratory.

The solar reflectance of roofing samples was measured following ASTM Standard C1549 with a solar spectrum reflectometer (Version 6, Devices & Services, Dallas TX), using an air mass 1 global horizontal (AM1GH) output provided by the manufacturer. Eight measurements at non-overlapping spots were made on each specimen, and reported as the mean ± standard deviation.

2.2. Bench-scale tests

The bench-scale chamber test used in this study has been described in our previous work [9,10] and followed the conditions stipulated by ISO

Standard 22197-1. Briefly, the tested specimen sat inside an air-tight flow reaction chamber, receiving irradiation through a quartz window from a UV-A lamp with maximum intensity at about 360 nm (Model TL-D, Actinic BL, Philips, Andover, MA). Irradiance was highest at the center of the specimen and consistent over the exposed surface, averaging 11.5 ± 1.5 W m^{-2}, as determined with a digital radiometer (Model UVX, UVP LLC, Upland, CA). Air flow of 3 L min^{-1} enriched with NO (g) was introduced into the chamber at 50% relative humidity (RH). The NO target concentration of 1,000 ppb was achieved by diluting with air a 50 ppm NO flow from a pre-mixed cylinder (Praxair, Danbury, CT). Downstream of the system, a chemiluminescent NO_x analyzer (Model 200A, Teledyne Technologies, Thousand Oaks, CA) was used to record in real time the concentrations of NO and NO_2 present in the air at the chamber's outlet. Air temperature and RH at the outlet was measured using an in-line digital HIH6100 series T/RH sensor (Honeywell, Charlotte, NC), prior to venting in a fume hood. The gap between the tested specimen and the quartz window was 5 mm. The chamber surface temperature was kept at 55 ± 3 °C using an external circulating bath, to simulate conditions that are close to those found on building surfaces under the sun.

2.3. Pilot-scale tests

The pilot-scale exposure system (Fig. 1) consisted of a rectangular stainless-steel main body topped with a UV-transparent film. The body dimensions were 153.6 cm L × 47.4 cm W × 11.5 cm H (60″ L × 18.5″ W × 4.5″ H). The top was covered with a fluorinated ethylene propylene (FEP) film of 51 μm (0.002") thickness. The UV transmission efficiency through the FEP film was tested with a UVA lamp at 365 nm and a digital radiometer, confirming that the film was not attenuating the UV light. The main body was connected to conical flanges on each side, ending in cylindrical ductwork at the inlet and outlet of the system. Two air sampling ports were installed on the transition flanges, collecting chamber air from about 6 cm above the surface. During the experiments, the specimens were placed in the middle of the exposure chamber, completely exposed to irradiation through the film. Experimental conditions used in this study are reported in Table 1.

2.3.1. Laboratory validation of the pilot-scale system

The pilot-scale chamber was tested in the laboratory by irradiating with two parallel 123 cm (48″) long UVA fluorescent lamps (40 W, Philips F40T12). The lamps were placed directly over the chamber at the desired height to obtain the same UV intensity (11.5 W m^{-2}) at the specimen surface as in the bench-scale chamber. NO (g) was diluted with air in a 100 L Teflon bag to achieve the desired target concentration. The diluted mixture was introduced into the chamber inlet opening using a peristaltic pump and ¼" Teflon tubing. Under high flow conditions, a large axial fan (8 cm × 8 cm) was placed approximately 5 cm inside the inlet flange, and pointed in different directions to create air flow either parallel or at an angle with respect to the chamber walls. NO-enriched air was admitted into the chamber through the fan. A low-flow

Table 1
Experimental setup and flow conditions in bench- and pilot-scale tests.

Scale	Location	Sample	Flow	Flow rate (L min^{-1})	Face velocity (m s^{-1})	Residence time (s)
Bench	Indoor	P25, BWC, BWP		3.0	0.10	1.8
Pilot	Indoor	P25	High	440	0.14	4.4
			Medium	292	9.0×10^{-2}	6.5
			Low	1.1	3.4×10^{-4}	1,800
		BWP[a]	High	440	0.14	4.4
			Low	1.1	3.4×10^{-4}	1,800
	Outdoor	BWP[a]	High	440	0.14	4.4
			Low	1.1	3.4×10^{-4}	1,800

[a] Activated through 75 days of outdoor exposure.

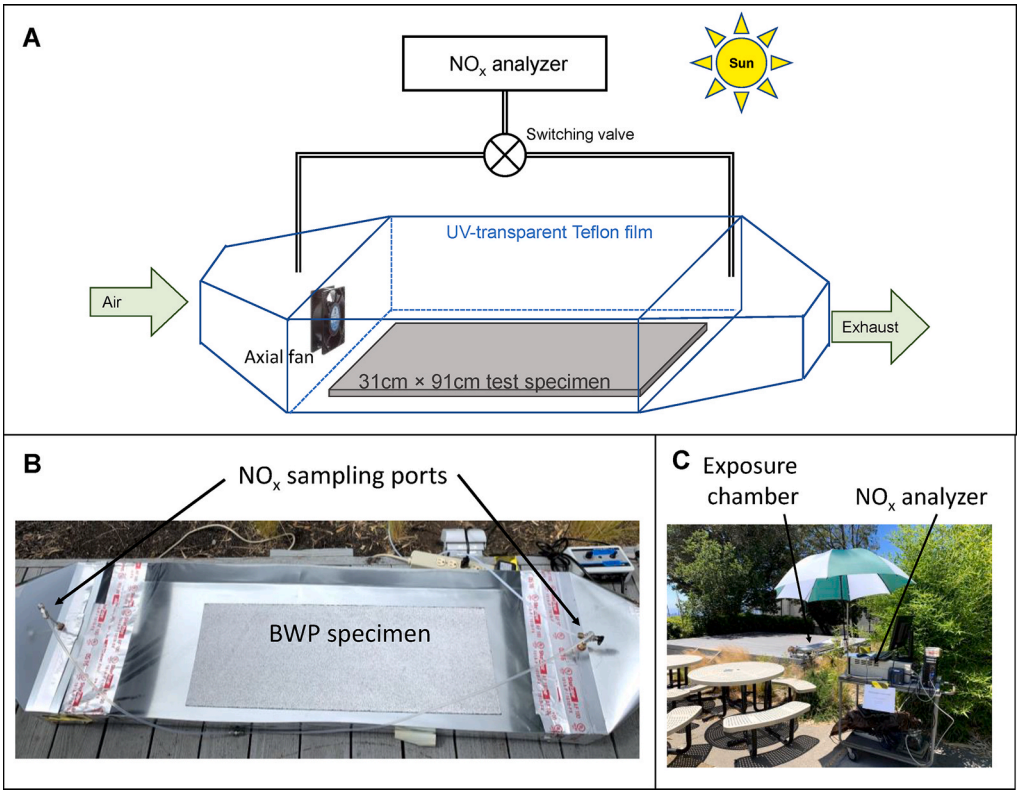

Fig. 1. (A) Schematic of experimental setup for pilot-scale tests. (B) Image of the specimen lying flat inside the chamber under solar irradiation. (C) NO_x analyzer, ancillary equipment, and computer for data logging were set up on a cart.

condition was tested by introducing three small axial fans (4 cm × 4 cm) at different angles with respect to the chamber wall. The air flow rate inside the chamber during each high flow experiment was determined by measuring air flow velocity (expressed in m s^{-1}) at the outlet opening (10 cm diameter) with an anemometer, then converting to flow rate (L min^{-1}) by multiplying it by the outlet opening area. Air flow rate during the low-flow experiments was determined directly from the injection rate of NO-enriched air. NO_x concentration was measured through the downstream sampling port. Prior to irradiation, it was confirmed that NO levels measured at upstream and downstream ports matched within a variance of ±10%. The chamber exhaust was directed to a fume hood. All laboratory tests were carried out at room temperature (20–25 °C).

2.3.2. Pilot-scale measurements in the outdoor environment

The outdoor experimental site was an elevated wooden platform adjacent to the laboratory building at LBNL in Berkeley, CA. It is depicted in Fig. 1. The pilot-scale chamber was placed on the platform, under direct sunlight between 9 a.m. and 5 p.m., local standard time. An opaque plastic cover was used during "dark" periods in which sunlight was avoided, to better quantify the photocatalytic effect. The NO_x analyzer, sampling pump, and computer for data logging were installed on a utility cart placed at 2 m from the platform. Due to the low NO_x concentration in ambient air, supplemental NO or NO_2 was introduced into the chamber from 100-L Teflon bags, injecting the NO_x-enriched air into the exposure chamber with a peristaltic pump. Challenge NO concentration entering the chamber was 100–200 ppb. The inlet and outlet of the chamber were covered with cardboard shields to prevent wind from causing flow fluctuations inside the chamber. The same digital radiometer (UVX) was used to determine the UV irradiance during each experiment. In addition, a Kipp & Zonen SP Lite2 Silicon Pyranometer connected to an Omega OM-DAQPRO-5300 data logger was used to measure the solar irradiance in a sub-set of experiments.

3. Calculations

The test performed with each specimen comprised one or more cycles of the following three segments, all under a constant flow of air enriched with NO or with a NO/NO_2 mixture:

a) pre-equilibration in the dark of about 1 h duration for bench-scale chamber experiments, and 15–30 min for pilot-scale experiments;
b) continuous UV (laboratory) or solar (outdoor) irradiation. The duration was about 6 h for bench-scale chamber experiments and 0.8–2 h for pilot-scale outdoor experiments; and
c) post-equilibration in the dark, of comparable duration as the pre-equilibration periods. In outdoor tests, this period also served as pre-equilibration for the next irradiation cycle.

The challenge NO and NO_2 concentrations were measured during the pre- and post-equilibration periods. The incoming concentration during the UV irradiation period ($c_{NO_{in}}$ and $c_{NO_{2_{in}}}$) was calculated as the average of the corresponding pre- and post-equilibration concentrations. In experiments where NO was the challenge gas, the NO removal rate (r_{NO}, expressed in mol h^{-1}), and the NO_2 rate of formation from NO oxidation (r_{NO_2}, also expressed in mol h^{-1}) were calculated using the difference between the inlet and outlet concentrations of NO and NO_2:

$$r_{NO} = \frac{\int_0^\tau n_{NO_{removed}}(t)\,dt}{\tau} = \frac{\int_0^\tau [c_{NO_{in}} - c_{NO_{out}}(t)]dt}{\tau} \times \frac{Q}{V_n} \quad (1)$$

$$r_{NO_2} = \frac{\int_0^\tau n_{NO_{2\,formed}}(t)\,dt}{\tau} = \frac{\int_0^\tau \left[c_{NO_{2_{out}}}(t) - c_{NO_{2_{in}}}\right] dt}{\tau} \times \frac{Q}{V_n} \quad (2)$$

where Q is the air flow rate, τ is duration of irradiation, t is time, n is the number of moles, and V_n is the normalized gas volume for 1 mol of gas at standard pressure and room temperature. The NO_x deposition rate (R_{NO_x}, expressed in μmol h^{-1} m^{-2}) was calculated as the difference between NO removal and NO_2 formation rates per unit area (A):

$$R_{NO_x} = \frac{r_{NO} - r_{NO_2}}{A} \quad (3)$$

In experiments where NO_2 was the challenge gas, R_{NO_x} was calculated similarly, by subtracting the rate of NO formation from the removal rate of NO_2. The exposed surface area was $A = 0.02$ m^2 for small specimens used in bench-scale chamber experiments, and $A = 0.27$ m^2 for large specimens used in pilot-scale experiments.

In experiments where NO was the challenge compound, the NO deposition velocity $v_{d(NO)}$ was defined as the flux of NO to the specimen surface divided by the free stream concentration. In the chamber there was no other reactive material besides the sample specimen. At steady state, the deposition velocity was calculated as [34,35]:

$$v_{d(NO)} = \frac{Q}{A \times c_{NO_{out}}}(c_{NO_{in}} - c_{NO_{out}}) \quad (4)$$

As the measured deposition velocity may be different under various flow conditions, the reported values are specific to the conditions discussed in this study.

4. Results and discussion

4.1. Solar reflectance of fresh and aged samples

Small specimens for bench-scale testing were exposed in the field for a total of 22 months (March 2020 through January 2022), with individual specimen retrieved at 115 days (2020-06-29), 235 days (2020-10-26), 12 months (2021-03-26), and 22 months (2022-01-05). Fig. 2 presents the solar reflectance (SR) measured for the retrieved BWP and BWC samples. Overall, both materials retained most of their high initial reflectance over the entire exposed period, with the SR of BWP dropping from 0.598 to 0.573 (4% of the initial value) at the end of 22-month exposure, and the SR of BWC specimen increasing from 0.562 to 0.574 (2% of the initial value). These changes, and the overall fluctuations observed over the 22-month period, are of the same magnitude as the relative standard deviation of the measurements. The lowest SR values were observed after 235 days of exposure under almost five months of dry weather (Jun to Nov 2020); these were <6% lower than the initial SRs, suggesting good self-cleaning by both bright white shingle specimens regardless of their photocatalytic activity.

4.2. De-NO_x efficiency measured in bench-scale experiment

The P25-coated plate, BWP, and BWC specimens were tested in the bench-scale chamber, under a 3 L min^{-1} flow of 1000 ppb NO, with a surface temperature of 55 °C. Results are presented in Fig. 3. The BWC

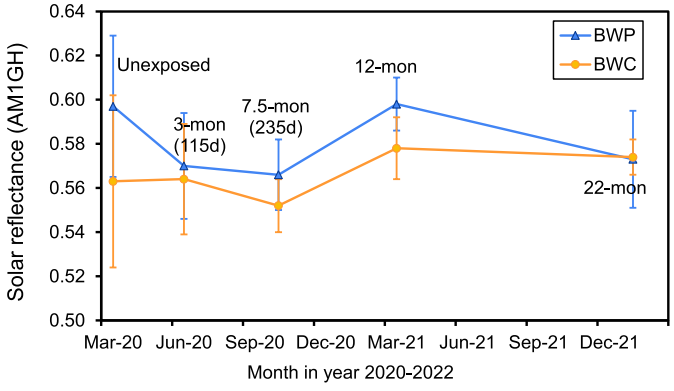

Fig. 2. Measured solar reflectance of the BWP and BWC specimens before and during natural exposure in the period March 2020–January 2022.

sample was observed to show minimal (though not negligible) photocatalytic activity, while the BWP sample exhibited de-NO_x properties. The NO abatement and NO_2 formation rates were lower for BWP than for P25, but the NO_x removal efficiency of the BWP sample was comparable to that of the P25-coated plate, with $R_{NO_x} = 17 \pm 1$ μmol h^{-1} m^{-2} for the unexposed BWP sample, and $R_{NO_x} = 18 \pm 1$ μmol h^{-1} m^{-2} for P25. Exposure of BWP specimens for 116 days led to reductions in NO and NO_2 reaction rates, and NO_x deposition rates. A longer exposure period of 235 days led to further loss of NO reactivity which, combined with a higher NO_2 yield, resulted in a decreased NO_x deposition rate. These results are consistent with those observed for aged photocatalytic PTFE-coated fiberglass architectural fabrics, which also lost some NO_x-abatement performance while retaining their initial solar reflectance practically unchanged [10]. The NO_x removal efficiency and NO deposition velocity of the BWP specimen slightly recovered at the end of the 12-month exposure, most likely resulting from the 17 cm precipitation accumulated between Dec 2020 and Mar 2021, before the specimen was retrieved on 2021-03-26. In the following rainy season between Oct 2021 and Jan 2022, there was more than twice as much precipitation (39 cm) as in the previous year. This led to a full recovery of the BWP specimen's photocatalytic performance, with even higher NO_x removal efficiency and NO deposition velocity than the unexposed sample. These results highlight the retention of photocatalytic performance during almost two years of aging in the field, and the seasonal effects corresponding to partial loss of activity during the dry season and reactivation in the rainy season. This seasonal effect has been observed previously [9, 10].

4.3. De-NO_x efficiency measured in laboratory validation of pilot-scale experiment

The BWC and BWP samples were activated by exposure for 75 days during the rainy season (2020-03-05 to 2020-05-19), and tested in the pilot-scale chamber under controlled conditions at the laboratory, before being used in new outdoor exposure tests. Laboratory experiments were performed at room temperature (18–20 °C) and with a challenge NO concentration below 100 ppb. The P25-coated plate of the same dimensions was also tested in identical conditions, as a reference. The concentration of NO (and a low level of NO_2) in the supply air fluctuated slightly, caused by the presence of small amounts of NO_x in indoor air. The BWC sample did not present photocatalytic activity in these tests, likely due to the lower NO concentration with respect to the ISO 22197-1 test conditions used in the bench-scale tests described above.

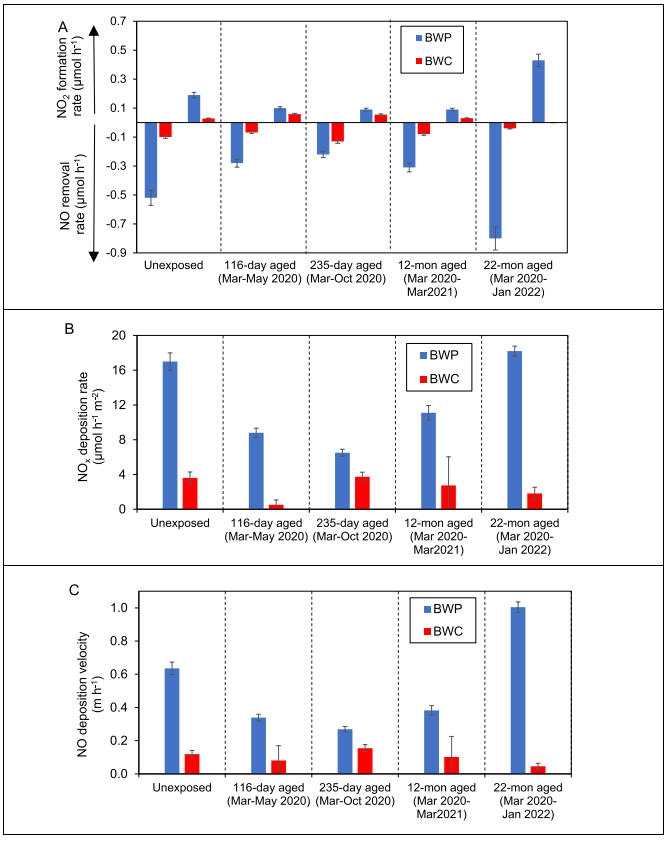

Fig. 3. Results of bench-scale tests, showing (A) NO removal and NO_2 formation rates, (B) NO_x deposition rate, and (C) NO deposition velocity.

4.3.1. P25-coated plate

The P25-coated specimen was tested in the laboratory under three flow conditions:

a) high flow (440 L min^{-1}), with the large axial fan aligned with the flow path from inlet to outlet;
b) medium flow (292 L min^{-1}), with the same fan pointing at an angle with respect to the flow path; and
c) low flow (1.1 L min^{-1}), in which the flow of NO-enriched air as the only supply air source, using three small mixing fans inside the chamber.

In Fig. 4A, the calculated NO_x deposition rates were plotted for three sequential replicates under each of the flow conditions. The P25-coated plate showed the highest NO_x deposition rate under the high flow condition (replicates H1, H2, and H3), with 100 ppb NO in the challenge air. For P25, average NO_x deposition rate was 7 times as high as that under the medium flow condition (replicates M1, M2, and M3), a much larger difference than the ratio of the flow rates. With the low air flow (replicates L1, L2, and L3), the same rate was more than one order of magnitude lower than those under the medium and high flow conditions. For P25, the first run within each set of three replicate tests showed the highest NO_x deposition rate, while subsequent runs were

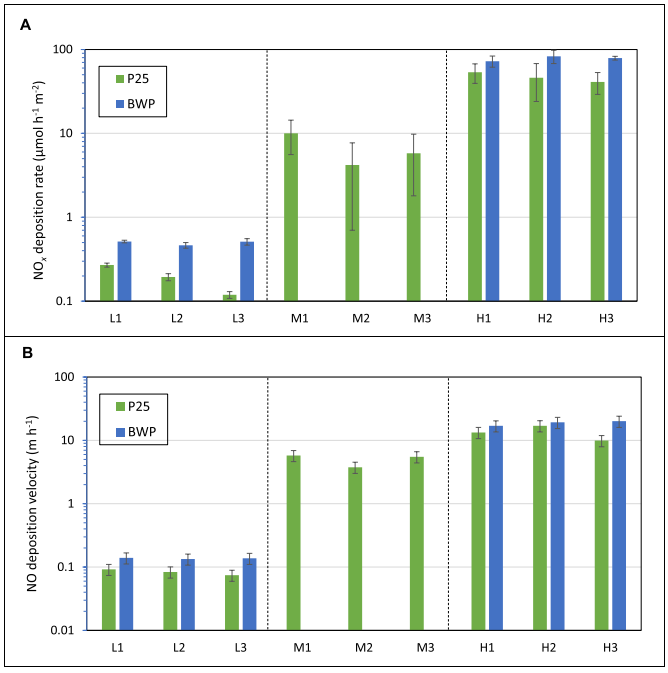

Fig. 4. (A) NO_x deposition rate, and (B) NO deposition velocity, each determined for a P25-coated plate (1.0 g m^{-2}) and the pre-activated BWP specimen in the pilot-scale chamber indoors under high (400 L min^{-1}), medium (292 L min^{-1}), and low (1.1 L min^{-1}) flow conditions.

lower, indicating partial inactivation of the tested specimen. This observation is consistent with our previously reported results [9].

Similar trends were observed in Fig. 4B for the NO deposition velocity. For P25, relative deviation between tests at high flow (H1, H2, H3) and medium flow (M1, M2, M3) was smaller, compared with that of NO_x deposition rate (Fig. 4A). The effect of material inactivation was not reflected in the NO deposition velocity, suggesting that this parameter is a more robust metric of performance.

4.3.2. BWP sample

The BWP specimen was tested in the laboratory at the above-mentioned high (440 L min^{-1}) and low (1.1 L min^{-1}) air flow rates. Three replicate determinations were made for each condition. The performance of the activated BWP material was always better than that of P25, as illustrated in Fig. 4. The NO_x deposition rate on BWP was, on average, 70% greater than the NO_x deposition on P25 at the high flow condition, and 160% greater at the low flow condition. The NO deposition velocity was 40%–60% higher on BWP with respect to P25. The BWP specimen did not show evidence of inactivation. The NO deposition velocity determined for each replicate was very reproducible, with a deviation <10%.

4.4. Outdoor pilot-scale measurements

Having validated the pilot-scale approach in the indoor setting, the following tests were performed using the same chamber outdoors, using exclusively the BWP sample.

4.4.1. BWP membrane challenged with NO

The pre-activated BWP specimen was tested with outdoor solar radiation, under high and low flow conditions. Fig. 5 illustrates the measured NO and NO_2 concentrations during irradiation and dark periods. In both low and high air flow rate experiments there was a formation of NO_2 as a consequence of the photocatalytic oxidation of NO. This is consistent with our observations in bench-scale and pilot-scale experiments.

Under both low and high flow conditions, the NO_x deposition rate of BWP measured outdoors was higher than those measured indoors for both BWP and P25, as shown in Fig. 6. The NO deposition velocity was comparable for BWP outdoors and indoors under low flow conditions, but it was greater outdoors when the system was operated at the higher air flow. The higher UV irradiance measured in the outdoor experiments is likely the reason for the observed higher photocatalytic activity. Fig. 7 shows the solar irradiance and UV irradiance (365 nm) measured next to the chamber during one of the outdoor experiments. Similar curves for other experiments are presented in Fig. S2 (Supporting Information). The UV irradiance outdoors was always higher than that used indoors. Significant fluctuations in outdoor irradiance are due to measurements being carried out at different times of day, and at days with different cloud coverage (or absence thereof). Fig. 8 illustrates a correlation between different outdoor measurements of NO deposition rate and the average UV irradiance during the corresponding sampling period. This effect was observed both in low and high air flow experiments.

When the system operated at the low flow conditions, the NO deposition rate was comparable indoors and outdoors, despite the higher outdoor irradiance. This may be due to the longer residence times achieved in the low flow tests, which were more than two orders of magnitude longer indoors than outdoors.

4.4.2. BWP membrane challenged with an NO/NO_2 mixture

In outdoor experiments, the NO_2 level was 18–50 ppb during the experiments with NO as the challenge compound. This is due to the presence of NO_2 in background outdoor air. In a separate set of experiments, an additional amount of NO_2 was added to NO reaching a NO_2 concentration of 110–140 ppb. This mixture allowed us to test the de-NO_x performance when both NO and NO_2 were present at higher concentrations. These tests were conducted under the low flow condition, with five periods of irradiation separated by periods in the dark, during a single day. Fig. 9 presents the NO and NO_2 concentration measured during the experiments.

As shown in Fig. 10, the first test showed significantly higher deposition velocity of both NO and NO_2. During the subsequent tests carried out during the day, the NO deposition velocity dropped to half of the initial value (0.24 m h^{-1}) and remained relatively stable. On the other hand, the NO_2 deposition velocity decreased with time, from 0.24 m h^{-1} to 0.02 m h^{-1} by the end of the five consecutive tests. This result is consistent with our previous observation that NO_2 is more sensitive to partial inactivation of the photocatalyst likely due to the formation of

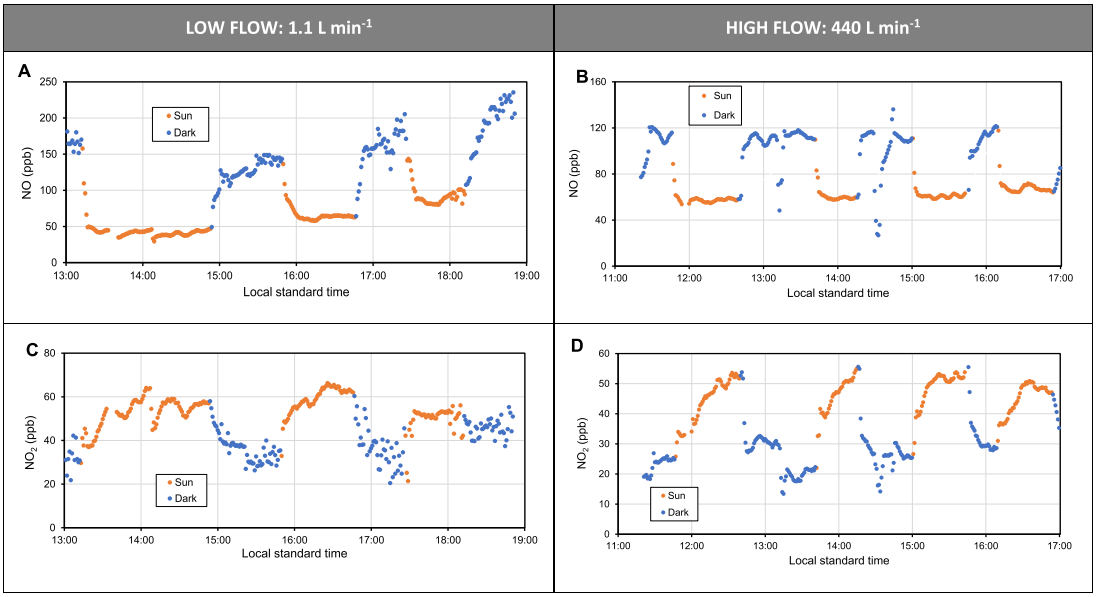

Fig. 5. NO_x concentration measured in outdoor experiments on 2020-06-25 (low flow) and 2020-06-26 (high flow), with NO as the main challenge gas. (A) NO concentration at low air flow; (B) NO concentration at high air flow; (C) NO_2 concentration at low air flow; (D) NO_2 concentration at high air flow.

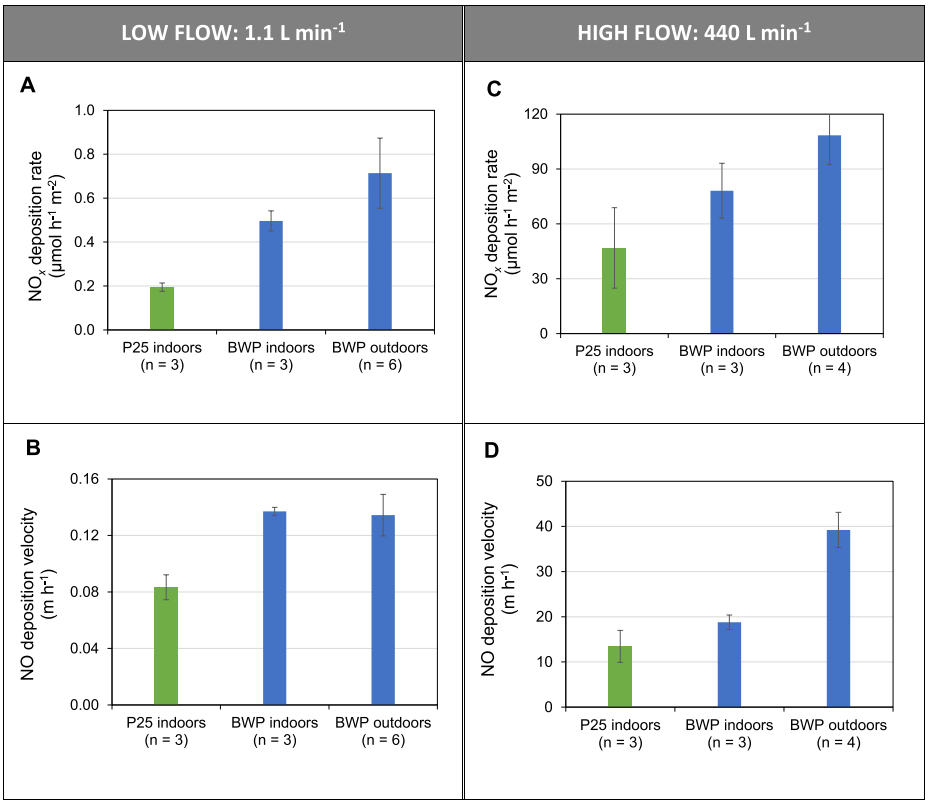

Fig. 6. Pilot-scale chamber results for BWP indoors and outdoors, compared with P25 indoors. (A) NO_x deposition rate at low air flow; (B) NO deposition velocity at low air flow; (C) NO_x deposition rate at high air flow; and (D) NO deposition velocity at high air flow.

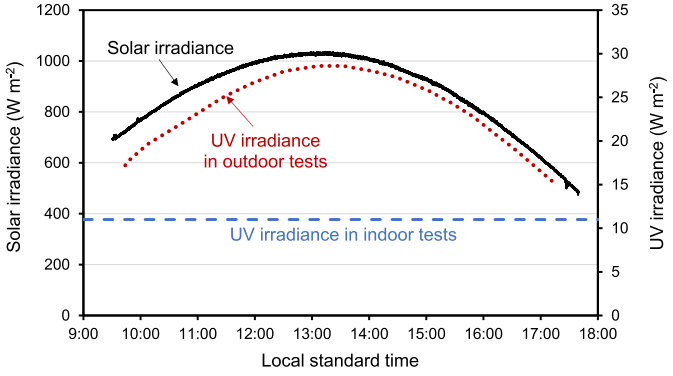

Fig. 7. Solar irradiance (black solid line) and UV irradiance @ 365 nm (red dotted line) measured during one outdoor experiment. The blue dashed line indicates the UV irradiance (11.5 W m^{-2}) in the bench scale experiment. (For interpretation of the references to colour in this figure legend, the reader is referred to the Web version of this article.)

surface bound species such as nitrate anions [9]. Fig. S3 (Supporting Information) illustrates the measured NO and NO_2 reaction rates and the NO_x deposition rate for the same tests.

5. Conclusions

The experiments showed that the BWP sample retained its photocatalytic activity and solar reflectance after 22 months of exposure in the field. The de-NO_x effect was observed under both a low (1 L min^{-1}) and high (440 L min^{-1}) air flow. The outdoor pilot-scale experiments confirmed that the photocatalytic de-NO_x process can proceed under conditions that resemble real-world exposure, with generally higher NO_x deposition rates than those measured in laboratory with the same

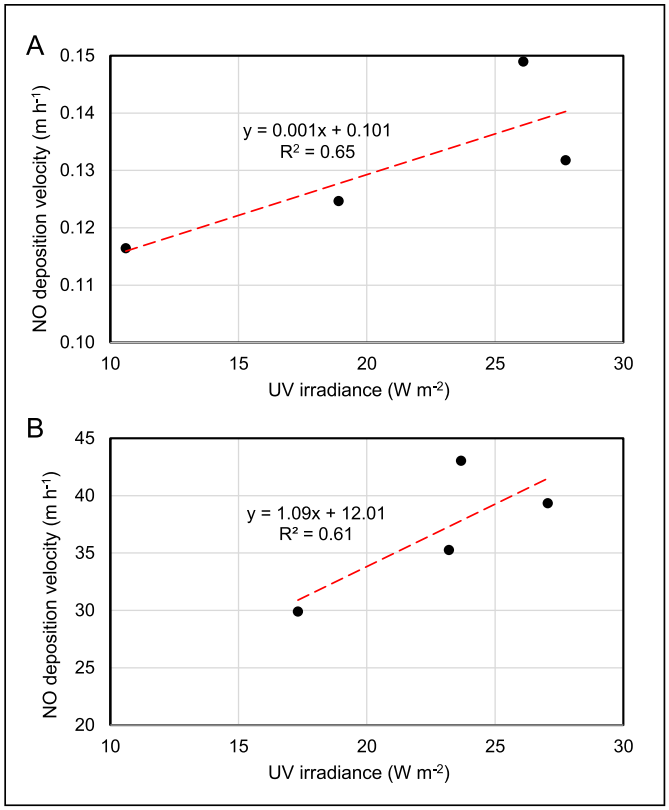

Fig. 8. NO deposition velocity onto BWP as a function of UV irradiance (W/m^2) in outdoor experiments carried out with (A) low air flow and (B) high air flow.

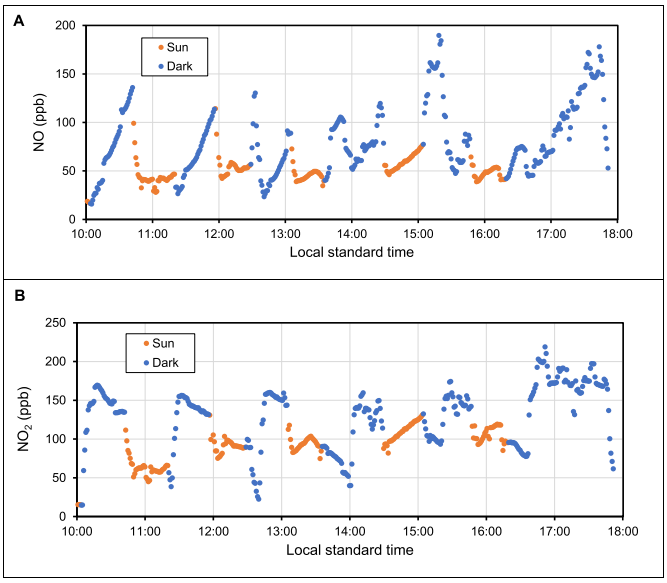

Fig. 9. (A) NO and (B) NO_2 concentrations measured during an outdoor experiment on 2020-06-30, with the BWP sample challenged with a NO/NO_2 mixture.

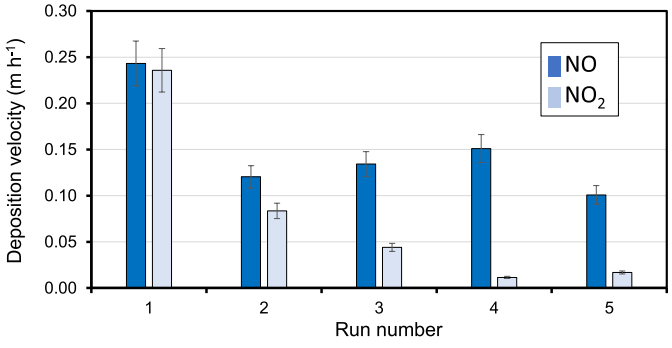

Fig. 10. Deposition velocity of NO and NO_2 measured in outdoor experiments using a NO/NO_2 mixture as the challenge gas. The flow rate was 1.1 L min^{-1}.

material due to higher outdoor UV irradiance. The pilot-scale test method incorporated conditions that have not been explored in standardized bench-scale methods, such as ambient air temperature, solar irradiance, and presence of NO_2; the results from the pilot-scale tests can support extrapolation to real-world conditions of results obtained with the ISO Standard 22197-1 or comparable bench-scale methods. It provides a simplified alternative to field campaigns, which could demonstrate performance of large-scale application of these materials, but often require substantial funding and effort (e.g., instrumentation, site access, and long-duration measurement). In the meantime, this test method is limited to air mixing within the reactor's height (11 cm), and was not able to evaluate photoactivity under low NO_x levels (<50 ppb) due to instrument detection limit. Therefore, 2D/3D street canyon or urban models consisting of buildings surfaces coupling urban turbulence/solar shading with photocatalytic roofing membrane are promising next steps to validate the real-world impact of these materials [36, 37].

CRediT authorship contribution statement

Xiaochen Tang: Writing – original draft, Visualization, Methodology, Investigation, Conceptualization. **Lara Ughetta:** Resources, Investigation, Conceptualization. **Rachael A.T. Gould:** Investigation. **Rebecca L.A. Everman:** Investigation. **Taisiya Skorina:** Investigation. **Sharon Chen:** Investigation. **Maureen Kavanagh:** Resources, Investigation, Conceptualization. **Ronnen Levinson:** Writing – review & editing, Methodology, Conceptualization. **Hugo Destaillats:** Writing – review & editing, Writing – original draft, Supervision, Methodology, Funding acquisition, Conceptualization.

Declaration of competing interest

The authors declare the following financial interests/personal relationships which may be considered as potential competing interests: Hugo Destaillats reports financial support was provided by 3M Company. Lara Ughetta, Rachael Gould, Rebecca Everman, Taisiya Skorina, Maureen Kavanagh reports a relationship with 3 M Company that includes: employment.

Data availability

Data will be made available on request.

Acknowledgements

This research was funded by the Industrial Mineral Products Division of the 3M Company under contract FP00002421. It was also supported by the Assistant Secretary for Energy Efficiency and Renewable Energy, U.S. Department of Energy under Contract No. DEAC02 - 05CH11231. The authors thank Randy Maddalena (LBNL) for his assistance in setting up outdoor measurements, and Lucia Cancelada for her participation in preliminary measurements.

Supporting Information.

Supporting information can be found online at https://doi.org/10.1016/j.solmat.2022.111907.

References

[1] C.F. Chen, Y.L. Wang, G.Q. Pan, Q.W. Wang, Gel-sol synthesis of surface-treated TiO_2 nanoparticles and incorporation with waterborne acrylic resin systems for clear UV protective coatings, J. Coating Technol. Res. 11 (2014) 785–791, https://doi.org/10.1007/s11998-014-9583-x.

[2] M.V. Diamanti, R. Paolini, M. Rossini, A.B. Aslan, M. Zinzi, T. Poli, M.P. Pedeferri, Long term self-cleaning and photocatalytic performance of anatase added mortars exposed to the urban environment, Construct. Build. Mater. 96 (2015) 270–278, https://doi.org/10.1016/j.conbuildmat.2015.08.028.

[3] M. Radeka, S. Markov, E. Loncar, O. Rudic, S. Vucetic, J. Ranogajec, Photocatalytic effects of TiO_2 mesoporous coating immobilized on clay roofing tiles, J. Eur. Ceram. Soc. 34 (2014) 127–136, https://doi.org/10.1016/j.jeurceramsoc.2013.07.010.

[4] O. Rudic, D. Rajnovic, D. Cjepa, S. Vucetic, J. Ranogajec, Investigation of the durability of porous mineral substrates with newly designed TiO_2-LDH coating, Ceram. Int. 41 (2015) 9779–9792, https://doi.org/10.1016/j.ceramint.2015.04.050.

[5] D. Colangiuli, M. Lettieri, M. Masieri, A. Calia, Field study in an urban environment of simultaneous self-cleaning and hydrophobic nanosized TiO_2-based coatings on stone for the protection of building surface, Sci. Total Environ. 650 (2019) 2919–2930, https://doi.org/10.1016/j.scitotenv.2018.10.044.

[6] M.V. Diamanti, M. Ormellese, M.P. Pedeferri, Characterization of photocatalytic and superhydrophilic properties of mortars containing titanium dioxide, Cement Concr. Res. 38 (2008) 1349–1353, https://doi.org/10.1016/j.cemconres.2008.07.003.

[7] A. Folli, C. Pade, T.B. Hansen, T. De Marco, D.E. Macphee, TiO_2 photocatalysis in cementitious systems: insights into self-cleaning and depollution chemistry, Cement Concr. Res. 42 (2012) 539–548, https://doi.org/10.1016/j.cemconres.2011.12.001.

[8] G.L. Guerrini, Photocatalytic performances in a city tunnel in Rome: NO_x monitoring results, Construct. Build. Mater. 27 (2012) 165–175, https://doi.org/10.1016/j.conbuildmat.2011.07.065.

[9] X. Tang, L. Ughetta, S.K. Shannon, S. Houzé de l'Aulnoit, S.S. Chen, R.A.T. Gould, M.L. Russell, J. Zhang, G. Ban-Weiss, R.L.A. Everman, F.W. Klink, R.M. Levinson, H. Destaillats, De-pollution efficacy of photocatalytic roofing granules, Build. Environ. 160 (2019), 106058, https://doi.org/10.1016/j.buildenv.2019.03.056.

[10] X. Tang, O. Rosseler, S. Chen, S. Houzé de l'Aulnoit, M.J. Lussier, J. Zhang, G. Ban Weiss, H.E. Gilbert, R. Levinson, H. Destaillats, Self-cleaning and de-pollution efficacies of photocatalytic architectural membranes, Appl. Catal. B Environ. 281 (2021), 119260, https://doi.org/10.1016/j.apcatb.2020.119260.

[11] A. Strini, S. Cassese, L. Schiavi, Measurement of benzene, toluene, ethylbenzene and o-xylene gas phase photodegradation by titanium dioxide dispersed in cementitious materials using a mixed flow reactor, Appl. Catal. B Environ. 61 (2005) 90–97, https://doi.org/10.1016/j.apcatb.2005.04.009.
[12] P. Krishnan, M.-H. Zhang, Y. Cheng, D.T. Riang, L.E. Yu, Photocatalytic degradation of SO_2 using TiO_2-containing silicate as a building coating material, Construct. Build. Mater. 43 (2013) 197–202, https://doi.org/10.1016/j.conbuildmat.2013.02.012.
[13] C. Garlisi, G. Palmisano, Radiation-free superhydrophilic and antifogging properties of e-beam evaporated TiO_2 films on glass, Appl. Surf. Sci. 420 (2017) 83–93, https://doi.org/10.1016/j.apsusc.2017.05.077.
[14] K.F. Salama, M. Zafar, Purification of ambient air by novel green plant with titanium dioxide nanoparticles, Int. J. Prev. Med. 13 (2022) 67, https://doi.org/10.4103/ijpvm.IJPVM_586_20.
[15] J. Morin, A. Gandolfo, B. Temime-Roussel, G. Brochard, V. Bergé, S. Gligorovski, H. Wortham, Key parameters influencing the uptake of m-xylene on photocatalytic paints, Build. Environ. 179 (2020), 106979, https://doi.org/10.1016/j.buildenv.2020.106979.
[16] D. Kotzias, V. Binas, G. Kiriakidis, Smart surfaces: photocatalytic degradation of priority pollutants on TiO_2-based coatings in indoor and outdoor environments-principles and mechanisms, Materials (Basel, Switzerland) 15 (2022), https://doi.org/10.3390/ma15020402.
[17] M.R. Hoffmann, S.T. Martin, W. Choi, D.W. Bahnemann, Environmental applications of semiconductor photocatalysis, Chem. Rev. 95 (1995) 69–96, https://doi.org/10.1021/cr00033a004.
[18] S. Ghosh, R. Patra, D. Majumdar, K. Sen, Developing scenario of titania-based building materials for environmental remediation, Int. J. Environ. Sci. Technol. 18 (2021) 2077–2102, https://doi.org/10.1007/s13762-020-02952-1.
[19] V. Binas, D. Venieri, D. Kotzias, G. Kiriakidis, Modified TiO_2 based photocatalysts for improved air and health quality, J. Materiomics 3 (2017) 3–16, https://doi.org/10.1016/j.jmat.2016.11.002.
[20] G.E. Kyriakodis, M. Santamouris, Using reflective pavements to mitigate urban heat island in warm climates - results from a large scale urban mitigation project, Urban Clim. 24 (2018) 326–339, https://doi.org/10.1016/j.uclim.2017.02.002.
[21] T. Ihara, Y. Kikegawa, K. Asahi, Y. Genchi, H. Kondo, Changes in year-round air temperature and annual energy consumption in office building areas by urban heat-island countermeasures and energy-saving measures, Appl. Energy 85 (2008) 12–25, https://doi.org/10.1016/j.apenergy.2007.06.012.
[22] M. Santamouris, A. Synnefa, T. Karlessi, Using advanced cool materials in the urban built environment to mitigate heat islands and improve thermal comfort conditions, Sol. Energy 85 (2011) 3085–3102, https://doi.org/10.1016/j.solener.2010.12.023.
[23] R. Levinson, G. Ban-Weiss, P. Berdahl, S. Chen, H. Destaillats, N. Dumas, H. Gilbert, H. Goudey, S. Houzé de l'Aulnoit, J. Kleissl, B. Kurtz, Y. Li, Y. Long, A. Mohegh, N. Nazarian, M. Pizzicotti, P. Rosado, M. Russell, J. Slack, X. Tang, J. Zhang, W. Zhang, Solar-reflective "cool" walls: benefits, Technologies, and implementation (CEC-500-2019-040; also LBNL-2001296), California Energy Commission, 2019, https://doi.org/10.20357/B7SP4H.
[24] ISO, Standard 22197-1, Fine Ceramics (Advanced Ceramics, Advanced Technical Ceramics) – Test Method for Air-Purification Performance of Semiconducting Photocatalytic Materials, International Organization for Standardization, 2016. Part 1. Removal of nitric oxide, https://www.iso.org/standard/65416.html.
[25] R. Dillert, J. Stotzner, A. Engel, D.W. Bahnemann, Influence of inlet concentration and light intensity on the photocatalytic oxidation of nitrogen(II) oxide at the surface of Aeroxide(R) TiO_2 P25, J. Hazard Mater. 211–212 (2012) 240–246, https://doi.org/10.1016/j.jhazmat.2011.11.041.
[26] Q.L. Yu, Y. Hendrix, S. Lorencik, H.J.H. Brouwers, Field study of NO_x degradation by a mineral-based air purifying paint, Build. Environ. 142 (2018) 70–82, https://doi.org/10.1016/j.buildenv.2018.06.014.
[27] R. Han, R. Andrews, C. O'Rourke, S. Hodgen, A. Mills, Photocatalytic air purification: effect of HNO_3 accumulation on NO_x and VOC removal, Catal. Today 380 (2021) 105–113, https://doi.org/10.1016/j.cattod.2021.04.017.
[28] A. Mills, R. Han, C. O'Rourke, S. Hodgen, Supersensitive test of photocatalytic activity based on ISO 22197-1:2016 for the removal of NO, J. Photochem. Photobiol. Chem. 400 (2020), 112734, https://doi.org/10.1016/j.jphotochem.2020.112734.
[29] F. Sieland, N.A.T. Duong, J. Schneider, D.W. Bahnemann, Influence of inorganic additives on the photocatalytic removal of nitric oxide and on the charge carrier dynamics of TiO_2 powders, J. Photochem. Photobiol. Chem. 366 (2018) 142–151, https://doi.org/10.1016/j.jphotochem.2018.01.036. SI.
[30] A. Mills, L. Burns, C. O'Rourke, S. Elouali, Kinetics of the photocatalysed oxidation of NO in the ISO 22197 reactor, J. Photochem. Photobiol. Chem. 321 (2016) 137–142, https://doi.org/10.1016/j.jphotochem.2016.01.010.
[31] B. Ohtani, O.O. Prieto-Mahaney, D. Li, R. Abe, What is Degussa (Evonik) P25? Crystalline composition analysis, reconstruction from isolated pure particles and photocatalytic activity tests, J. Photochem. Photobiol. Chem. 216 (2–3) (2010) 179–182, https://doi.org/10.1016/j.jphotochem.2010.07.024.
[32] F. Bai, R.A.T. Gould, M.T.M. Anderson, Photocatalytic coating, US Patent 8 (2015) 993, 471 B2, https://patents.google.com/patent/US8993471B8993472/en.
[33] J.L.M. Jacobs, Photocatalytic composition and method for preventing algae growth on building materials, US Patent 6 (2005) 881. https://patents.google.com/patent/US6881701, 701 B2.
[34] B.K. Coleman, H. Destaillats, A.T. Hodgson, W.W. Nazaroff, Ozone consumption and volatile byproduct formation from surface reactions with aircraft cabin materials and clothing fabrics, Atmos. Environ. 42 (2008) 642–654, https://doi.org/10.1016/j.atmosenv.2007.10.001.
[35] G.C. Morrison, W.W. Nazaroff, The rate of ozone uptake on carpets: experimental studies, Environ. Sci. Technol. 34 (2000) 4963–4968, https://doi.org/10.1021/es001361h.
[36] G. Chen, X. Yang, H. Yang, J. Hang, Y. Lin, X. Wang, Q. Wang, Y. Liu, The influence of aspect ratios and solar heating on flow and ventilation in 2D street canyons by scaled outdoor experiments, Build. Environ. 185 (2020), 107159, https://doi.org/10.1016/j.buildenv.2020.107159.
[37] T. Chen, H. Yang, G. Chen, C.K.C. Lam, J. Hang, X. Wang, Y. Liu, H. Ling, Integrated impacts of tree planting and aspect ratios on thermal environment in street canyons by scaled outdoor experiments, Sci. Total Environ. 764 (2021), 142920, https://doi.org/10.1016/j.scitotenv.2020.142920.